



**HAL**  
open science

## Non-Hermitian delocalization in a 2D photonic quasicrystal

Zhaoyang Zhang, Shun Liang, Ismaël Septembre, Jiawei Yu, Yongping Huang, Maochang Liu, Yanpeng Zhang, Min Xiao, Guillaume Malpuech, Dmitry Solnyshkov

► **To cite this version:**

Zhaoyang Zhang, Shun Liang, Ismaël Septembre, Jiawei Yu, Yongping Huang, et al.. Non-Hermitian delocalization in a 2D photonic quasicrystal. *Physical Review Letters*, 2024, 132 (26), pp.263801. 10.1103/PhysRevLett.132.263801 . hal-04675086

**HAL Id: hal-04675086**

**<https://hal.science/hal-04675086v1>**

Submitted on 22 Aug 2024

**HAL** is a multi-disciplinary open access archive for the deposit and dissemination of scientific research documents, whether they are published or not. The documents may come from teaching and research institutions in France or abroad, or from public or private research centers.

L'archive ouverte pluridisciplinaire **HAL**, est destinée au dépôt et à la diffusion de documents scientifiques de niveau recherche, publiés ou non, émanant des établissements d'enseignement et de recherche français ou étrangers, des laboratoires publics ou privés.

# Non-Hermitian delocalization in a 2D photonic quasicrystal

Zhaoyang Zhang,<sup>1,\*</sup> Shun Liang,<sup>1</sup> Ismael Septembre,<sup>2</sup> Jiawei Yu,<sup>1</sup> Yongping Huang,<sup>1</sup> Maochang Liu,<sup>3</sup> Yanpeng Zhang,<sup>1</sup> Min Xiao,<sup>4,5</sup> Guillaume Malpuech,<sup>2,†</sup> and Dmitry Solnyshkov<sup>2,6,‡</sup>

<sup>1</sup>*Key Laboratory for Physical Electronics and Devices of the Ministry of Education & Shaanxi Key Lab of Information Photonic Technique, School of Electronic Science and Engineering, Faculty of Electronics and Information, Xi'an Jiaotong University, Xi'an 710049, China*

<sup>2</sup>*Institut Pascal, PHOTON-N2, Université Clermont Auvergne, CNRS, Clermont INP, F-63000 Clermont-Ferrand, France*

<sup>3</sup>*International Research Center for Renewable Energy & State Key Laboratory of Multiphase Flow in Power Engineering, Xi'an Jiaotong University, Xi'an 710049, China*

<sup>4</sup>*Department of Physics, University of Arkansas, Fayetteville, Arkansas, 72701, USA*

<sup>5</sup>*National Laboratory of Solid State Microstructures and School of Physics, Nanjing University, Nanjing 210093, China*

<sup>6</sup>*Institut Universitaire de France (IUF), 75231 Paris, France*

Theoretical and experimental studies suggest that both Hermitian and non-Hermitian quasicrystals show localization due to the fractal spectrum and to the transition to diffusive bands via exceptional points, respectively. Here, we present an experimental study of a dodecagonal photonic quasicrystal based on electromagnetically-induced transparency in a Rb vapor cell. First, we observe the suppression of the wavepacket expansion in the Hermitian case. We then discover a new regime, where increasing the non-Hermiticity leads to delocalization, demonstrating that the behavior in non-Hermitian quasicrystal is richer than previously thought.

Quasicrystals are characterized by long-range order without translational symmetry [1]. In mathematics, they correspond to infinite non-periodic tilings. They can possess rotational symmetries incompatible with the translational one, such as the famous pentagonal symmetry of the Penrose tiling [2]. Another interesting and important case is the dodecagonal symmetry [3–5], which can be obtained from a superposition of two honeycomb lattices [6–9] rotated by  $30^\circ$ . This configuration is particularly timely, because of the extreme popularity of moiré honeycomb lattices, such as magic-angle twisted bilayer graphene [10], obtained for angles of rotation smaller than  $30^\circ$ . Moiré lattices and quasicrystals share many common properties, such as the presence of flat bands [11–13] in their spectrum. Dodecagonal quasicrystals are studied in many fields: chemistry [14–17], material science [4, 18, 19], electronics [8], topological physics [20–22], and photonics [7, 23–31].

For 1D quasicrystals or quasiperiodic lattices, many important analytical results were obtained using the Aubry-André model [32]: instead of considering a structure without translational symmetry in the positions of individual sites, one considers a periodic lattice with an incommensurate on-site potential of a variable strength [33–36]. It is now theoretically established and experimentally demonstrated that the dispersion of such a 1D quasicrystal contains an infinite number of gaps which obey the gap labeling theorem [37–40]. Each single band is infinitely narrow (flat), and the mobility of the particles filling the bands is strongly suppressed [33, 41]. This model allows studying the transition towards the fractal energy spectrum and the associated localization [42], driven by the variable strength

of the on-site potential.

2D quasicrystals have also been studied theoretically using the Aubry-André approach [13], namely considering a superposition of two lattices: one lattice is fixed, while the strength of the second lattice is varied, allowing to observe the modification of the transport. Another theoretical approach was to start directly with a quasicrystal potential and vary its strength relative to the recoil energy [43–46], allowing to see the localization of some of the eigenstates described by their inverse participation ratio. The bands tend to a Cantor set analogue [47], as in 1D [48]. In experiments with Hermitian 2D quasicrystals, phononic [49] and photonic [50] bandgaps were explicitly observed, in particular in dodecagonal structures [25]. Localization in photonic quasicrystals of different symmetries has been demonstrated very recently [51], and also the enhancement of the transport by disorder [52].

The potential can also be imaginary, making possible non-Hermitian phenomena analogous to the PT-symmetry-breaking transition, well-known in modern photonics [53]. Such transition has recently been predicted [36] and observed experimentally [54] in a 1D quasicrystal: increasing the non-Hermiticity induces a phase transition, which ultimately suppresses the mobility edge. All states become localized, and the mechanism is not due anymore to the quasi-crystal flat bands, but to the emergence of diffusive non-Hermitian bands (Fermi arcs limited by exceptional points). The Aubry-André approach has often been used for non-Hermitian systems [55–57]. Theoretical analyses of 2D systems have also been performed, based on a specific complex potential case [58], as the one considered in the 80s [59], with

results similar to 1D.

In this work, we take advantage of a reconfigurable photonic platform, atomic vapors under electromagnetically-induced transparency (EIT) [60] in a three-level atomic configuration [61–63], to perform an experimental study of a 2D Hermitian and non-Hermitian dodecagonal quasicrystals with a tunable ratio of intensities between the two honeycomb lattices forming the quasicrystal and a separately controllable non-Hermiticity. We demonstrate the localization transition with the increase of the intensity ratio of two lattices in the Hermitian case. On the contrary, in the non-Hermitian case the initial localization is followed by a delocalization. The latter is caused by the wavepacket redistribution due to the lifetime difference, occurring without crossing exceptional points.

The experimental scheme is shown in Fig. 1a. Two honeycomb photonic lattices are optically induced inside a Rb vapor cell by two hexagonal coupling beams  $\mathbf{E}_{C1}$  (frequency  $\omega_{c1}$ ) and  $\mathbf{E}_{C2}$  ( $\omega_{c2}$ ) with the same period of  $200 \mu\text{m}$ , injected into the vapor cell along the  $z$  direction (Fig. 1a is just a sketch, the experimental lattices are much larger). There exists a rotation angle (in the  $x-y$  plane) of  $30^\circ$  between the two hexagonal patterns. A weak Gaussian probe beam  $\mathbf{E}_p$  ( $\omega_p$ ) from a continuous-wave tunable laser co-propagates with coupling beams to excite a three-level atomic configuration (Fig. S1 in Supplementary [64]), where the well-known EIT effect can occur at appropriate detunings satisfying the two-photon resonance [60]  $\delta_p - \delta_{c1}(\delta_{c2}) = 0$ . The frequency detunings  $\delta_i$  ( $i = p, c1$  and  $c2$ ) are defined as the difference between the levels driven by laser field  $\mathbf{E}_i$  and its frequency (see [64]). Under the EIT condition, the susceptibility  $\chi$  experienced by  $\mathbf{E}_p$  is inversely related to the intensity of the coupling beams [65, 66]. The superposition intensity of two coupling beams is shown in Fig. 1b. Each coupling beam forms a single honeycomb photonic lattice (dark sites of the hexagonal pattern). The propagation of a probe beam through the vapor cell with an EIT-induced susceptibility distribution is described by the paraxial equation:

$$i \frac{\partial E}{\partial z} = -\frac{1}{2k_0} \Delta E - \frac{k_0 \chi}{2} E, \quad (1)$$

where  $k_0$  is the probe wave vector. This is equivalent to a 2D time-dependent Schrödinger equation with  $z \sim t$  (time),  $k_0 \sim m$  (particle mass), and  $\chi \sim -U$  (external potential). Susceptibility maxima (dark sites in Fig. 1b) thus correspond to potential minima.

The transmitted probe beam is received by a charge-coupled device camera (placed behind the output plane of the cell) through an imaging lens. During the experiment, the detuning of the probe beam is set as  $\delta_p = -260$  MHz, while  $\delta_{c1}$  and  $\delta_{c2}$  are manipulated [around positive two-photon detuning  $\delta_p - \delta_{c1}(\delta_{c2})$ ] to control the degree of non-Hermiticity of the induced photonic lattice (detun-

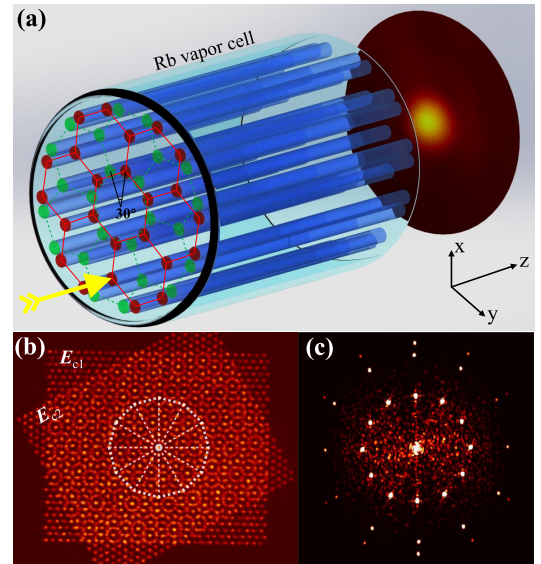


FIG. 1: a) Experimental scheme. b) The experimentally generated dodecagonal quasicrystal lattice formed by two hexagonal patterns rotated by  $30^\circ$ . c) Reciprocal-space image of the experimental quasicrystal lattice exhibiting a 12-fold symmetry in 3 orders of diffraction.

ings are in [64]). The 12-fold symmetry of the resulting lattice is underlined in Fig. 1b by the white dodecagon. Figure 1c shows the reciprocal-space image also exhibiting a 12-fold pattern with the first three diffraction orders clearly visible, which confirms the formation of a quasicrystal [8].

We study the evolution of the probe beam in the quasicrystal potential created by the coupling beams (under the limitations of the experimental method, see section I.C in [64]). The probe beam represents a narrow wavepacket (comparable to a single lattice site), its approximate injection point is shown by a yellow arrow in Fig. 1a. The duration of the time evolution in the 2D Schrödinger equation is fixed by the length of the vapor cell in the  $z$  direction. It is sufficient for the wavepacket to expand over several unit cells in a honeycomb lattice (its maximum is not necessarily at the injection point), whereas in the quasicrystal configuration the expansion is expected to be suppressed.

Figure 2 presents the results obtained in the fully Hermitian case. We keep one honeycomb lattice turned on with a constant intensity  $I_1$ , while varying the intensity  $I_2$  of the second lattice. The top panels Fig. 2a-c show the spatial distribution of the output probe patterns for three ratios of  $I_2/I_1$  (0, 0.4, 1, respectively). The cells of the two lattices are indicated in Fig. 2a,b with white and green dashed hexagons. Magenta dashed ellipses indicate the wavepacket width defined as the standard deviation, which is a square root of the second moment of the distribution (the variance). A clear narrowing of the output wavepacket can be observed. We note that it is perfectly

normal that the standard deviation of a multimodal distribution with different peak heights is smaller than the distance between these peaks [64, 67]. We have systematically studied the width of the output wavepacket as a function of the ratio  $I_2/I_1$ . The results are shown in Fig. 2d with black dots with error bars corresponding to the uncertainty of the extraction. For a full set of images see [64] or an online movie.

The output width of the wavepacket exhibits a continuous decrease (apart from a special localization point [68]) until it drops to its minimal size, approximately corresponding to the size of a single lattice site  $w_s$  that we take as a reference for this plot. To explain this behavior and to determine the transition point, we have performed numerical simulations based on Eq. (1) (see [64] for details). An example of the dispersion of a single honeycomb lattice is shown in Fig. 2e. It is plotted along the  $\Gamma K M K' \Gamma$  high-symmetry points. As expected [47, 48], the increase of  $I_2/I_1$  up to 1 opens a set of gaps in the dispersion, making the band similar to a Cantor set. An example of the dispersion for  $I_2/I_1 = 1$  is shown in Fig. 2f. It exhibits a lot of gaps separating narrowing bands. The density of states (DoS) allows us to detect and analyze full gaps. Figure 2g shows the DoS for the two cases shown in panels e and f: honeycomb lattice and dodecagonal quasicrystal. The Dirac point is visible for the honeycomb lattice (black) as a zero-DOS point with linear behavior in its vicinity. In the quasicrystal case (red), multiple large gaps accompanied by narrower secondary gaps are visible. The edges of each gap demonstrate van Hove singularities (DoS peaks).

The wavepacket expansion is determined by the group velocity of its components. If the wavepacket is narrow in real space, it covers the whole Brillouin zone and thus allows probing the *maximal* group velocity available. Our simulations show that the first (and largest) gap is opened precisely at the point of highest group velocity, because here the wavefunction is the most sensitive to the perturbing potential. It corresponds to the  $\Gamma K$  direction, where the dispersion of a single honeycomb lattice is given by  $E(k) = \pm J(1 + 2 \cos ka/2)$  in the tight-binding limit, and the group velocity is  $v_g(k) = \pm \hbar^{-1} J a \sin ka/2$ , with the maximal  $v_g$  point  $k_{max} = \pi/a$ . The gap size  $\Delta$  is linearly proportional to the strength of the incommensurate potential  $\lambda = I_2/I_1$  for small perturbations:  $\Delta \sim \lambda$ . This allows estimating the wavepacket expansion via the group velocity [64] as a function of the perturbation strength  $\lambda$ :

$$\frac{w(I_2/I_1)}{w_s} = 1 + A \sqrt{1 - B \left( \frac{I_2}{I_1} \right)^2}, \quad (2)$$

where  $A$  links the group velocity and the wavepacket width (including the effective propagation time), while  $B$  links the gap size  $\Delta$  and the perturbation  $\lambda$ . The red curve in Fig. 2d fits the experimental data with

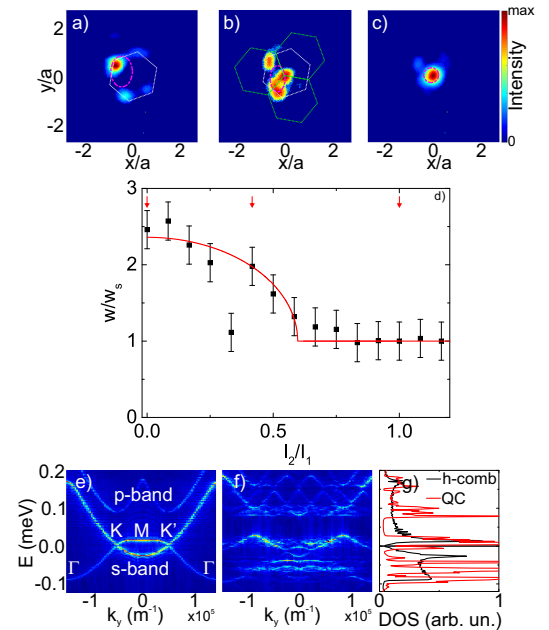


FIG. 2: Wavepacket expansion and the localization transition with the increase of the second lattice strength. a-c) Spatial images of the wavepacket after its evolution in the Hermitian lattice (lattice intensity ratio  $I_2/I_1 = 0, 0.4, 1$ , respectively), magenta line marks the wavepacket size. d) Wavepacket width  $w$  normalized by the lattice site width  $w_s$ . Red arrows mark the correspondence with panels a)-c). e) The dispersion of a single honeycomb lattice through  $\Gamma K M K' \Gamma$  points. f) The dispersion of a quasicrystal showing multiple gaps. g) The comparison of the DOS for a periodic honeycomb lattice and a quasicrystal. The gaps appear as zeroes of the DOS.

Eq. (2), giving the fitting parameters  $A \approx 1.35 \pm 0.09$  and  $B \approx 2.81 \pm 0.12$ . The value of  $A$  is directly determined by the wavepacket size at  $I_2 = 0$  in Fig. 2d. The value of  $B$  allows determining the localization transition point  $(I_2/I_1)_{loc} = \sqrt{1/B} \approx 0.597 \pm 0.013$ , of the same order of magnitude as in other quasicrystals [13]. We conclude that we have observed a localization transition for a Hermitian 2D dodecagonal quasicrystal and found its approximate position. The transition point depends on the particular periodic potential.

We now turn to the non-Hermitian case by changing the probe detuning. Indeed, the EIT configuration allows varying both real and imaginary parts of the effective potential via the complex susceptibility, potentially providing an important non-Hermiticity to the potential. It ultimately allows observing a transition similar to the PT-symmetry-breaking one [63], but we remain below this transition, defined by  $(\chi''/\chi')_{crit} \approx 0.4$ . Here,  $(\chi''/\chi') \approx 0.2$ . We fix the intensity  $I_1$  of the first honeycomb lattice and vary the other intensity  $I_2$ , with both lattices being non-Hermitian. We note that the real part of the potential is different from that of Fig. 2a-d.

Figure 3a-c shows the spatial images of the output

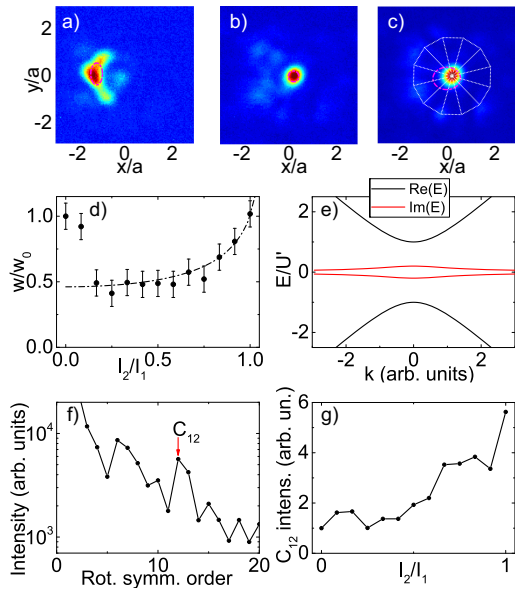


FIG. 3: Localization-delocalization transition in a 2D non-Hermitian quasicrystal. a)-c) Spatial images of the wavepacket after its evolution in the non-Hermitian lattice (lattice intensity ratio  $I_2/I_1 = 0.1, 0.4, 1$ , respectively). **Magenta line marks the wavepacket size.** d) Wavepacket width  $w$  normalized by the reference width  $w_0$  (corresponding to  $I_2/I_1 = 0$ ). Points with error bars (instrumental uncertainty) – experiment, dash-dotted line – theory. e) Real (black) and imaginary (red) parts of the eigenenergies of the weak complex potential model. f) Fourier-transform of the angular pattern of the panel c ( $I_2/I_1 = 1$ ) exhibiting a maximum corresponding to dodecagonal symmetry  $C_{12}$ . g) Intensity of the  $C_{12}$  maximum of the Fourier transform as a function of  $I_2/I_1$ : the symmetry of the wavepacket inherits that of the lattice.

beam for three values of  $I_2/I_1$  (0.1, 0.4, and 1, respectively). Interestingly, after the onset of localization, the wavepacket expansion is recovered almost completely, and the symmetry of the final wavepacket changes. Figure 3d shows the wavepacket size  $w$  (black dots) normalized by the size  $w_0$  observed for a single honeycomb lattice  $I_2/I_1 = 0$  (for a full set of images see [64] or an online movie). The measurements demonstrate first a rapid decrease and then an increase of the width, with a minimum around  $I_2/I_1 \approx 0.4$ .

To understand this behavior, we use the weak potential approximation and work with an effective Hamiltonian (see [64]). This allows us to obtain the asymptote shown in Fig. 3d with a black dash-dotted line. It describes the wavepacket broadening due to the non-Hermitian mechanism described by the following Hamiltonian:

$$H = \alpha(k - k_0)\sigma_z + U'\sigma_x + iU''\sigma_x. \quad (3)$$

This Hamiltonian exhibits exceptional points if  $U' = 0$ , that is, if the potential is purely imaginary. The position of exceptional points is determined by  $(k^* - k_0) = \pm U''/\alpha$ . In our case, they are not accessible, since

$U' \neq 0$ . Nevertheless, the non-Hermitian nature of the Hamiltonian leads to important consequences: the decay rate of the states starts to depend on their wave vector. The eigenvalues are given by  $E(k - k_0) = \pm \sqrt{U'^2(1 - i\lambda)^2 + \alpha^2(k - k_0)^2}$ . Figure 3e shows the corresponding correction to the overall decay rate. The resulting decay rate profile leads to the concentration of the wavepacket at longest-living states in the reciprocal space at the edge of the largest gap. Because of this, the wavepacket width in real space grows as a function of the ratio of the two lattices for fixed evolution time  $t$ , according to the following law [64]:

$$\Delta r = \frac{C}{\sqrt{1 - D \left(\frac{I_2}{I_1}\right)^2}}. \quad (4)$$

Figure 3d shows a fitting with  $C \approx 0.46 \pm 0.02$  (consistent with Fig. 2: the wavepacket expansion gives a factor  $C^{-1} \approx 2$  with respect to a single site) and  $D \approx 0.79 \pm 0.02$  (meaning that the characteristic decay length due to the non-Hermiticity is shorter than the vapor cell length [64], in agreement with the experiment). The theoretical curve presents a good agreement with the experimental data. We therefore conclude that while in periodic systems the non-Hermiticity can lead to localization via the PT-symmetry-breaking transition, in our quasicrystal we observe that the non-Hermiticity leads to delocalization in wavepacket expansion. We note that delocalization has been observed in pentagonal quasicrystals [52], but there it was induced by disorder and not by non-Hermiticity.

Contrary to the Hermitian case, where the wavepacket localization width is comparable to the size of a single lattice site  $w_s$ , the non-Hermitian case, thanks to the suppression of the localization, allows observing the wavepacket distribution over several neighboring sites for  $I_2/I_1 = 1$  (exact quasicrystal limit). We analyze the angular distribution of this wavepacket (the probability density averaged over the radial coordinate  $r$ ) by performing its Fourier transform (Fig. 3f). A clear maximum corresponding to the dodecagonal ( $C_{12}$ ) symmetry is observed. The corresponding dodecagon is marked in Fig. 3c with white dashed lines. This confirms that the wavepacket inherits the symmetry of the quasicrystal lattice. We also study the behavior of the  $C_{12}$  maximum of the angular Fourier transform with the intensity of the second lattice  $I_2/I_1$  in Fig. 3g (normalized to its "background" value at  $I_2/I_1 = 0$ ) and observe a strong growth of this component above  $I_2/I_1 \approx 0.6$ , when the wavepacket delocalization takes place. This confirms that for small intensity of the second lattice its effect can be seen as an incommensurate (effectively random) on-site potential for the initial (honeycomb) lattice, whereas for large intensities the superposition of two lattices must be indeed considered as a dodecagonal quasicrystal with associated properties.

To conclude, we have studied the beam evolution in a reconfigurable photonic platform, allowing us to continuously analyze the transition between a crystal and a quasicrystal both in Hermitian and non-Hermitian cases. We have observed an efficient localization of the beam in Hermitian quasicrystals. We have also shown that the combination of two localizing contributions (incommensurate potential and non-Hermiticity) can actually lead to delocalization, allowing us to recover almost the same transport properties as for a single periodic honeycomb Hermitian lattice, but with the wavepacket symmetry becoming dodecagonal. A similar non-Hermitian delocalization effect could also take place in moiré lattices. Our work can find direct applications for on-demand beam tailoring [69–71]. Generally speaking, the applications of quasicrystals in photonics go beyond the localization [50], waveguiding [72] and beam focusing [73]: in particular, they were also shown to exhibit negative refraction [26].

This work was supported by National Natural Science Foundation of China (No.51888103, No.62022066, and No.12074306) and European Union's Horizon 2020 program, through a FET Open research and innovation action under the grant agreement No. 964770 (Topo-Light). We also acknowledge the support of the ANR Labex Ganex (ANR-11-LABX-0014), and of the ANR program "Investissements d'Avenir" through the IDEX-ISITE initiative 16-IDEX-0001 (CAP 20-25).

---

\* Electronic address: zhyzhang@xjtu.edu.cn

† Electronic address: guillaume.malpuéch@uca.fr

‡ Electronic address: dmitry.solnyshkov@uca.fr

- [1] D. Levine and P. J. Steinhardt, *Phys. Rev. Lett.* **53**, 2477 (1984).
- [2] D. Shechtman, I. Blech, D. Gratias, and J. W. Cahn, *Phys. Rev. Lett.* **53**, 1951 (1984).
- [3] T. Ishimasa, H.-U. Nissen, and Y. Fukano, *Phys. Rev. Lett.* **55**, 511 (1985).
- [4] Q. Yang and W. Wei, *Phys. Rev. Lett.* **58**, 1020 (1987).
- [5] F. Gähler, in *Quasicrystalline materials : Proceedings of the I.L.L. / Codest Workshop, Grenoble, 21 - 25 March 1988*, edited by C. Janot (World Scientific, Singapore, 1988), chap. 7, pp. 272–284.
- [6] N. Niizeki and H. Mitani, *J. Phys. A: Math. Gen.* **20**, L405 (1987).
- [7] X. Zhang, Z.-Q. Zhang, and C. T. Chan, *Phys. Rev. B* **63**, 081105 (2001).
- [8] S. J. Ahn, P. Moon, T.-H. Kim, H.-W. Kim, H.-C. Shin, E. H. Kim, H. W. Cha, S.-J. Kahng, P. Kim, M. Koshino, et al., *Science* **361**, 782 (2018).
- [9] J. Crosse and P. Moon, *Sci. Rep.* **11**, 11548 (2021).
- [10] E. Y. Andrei and A. H. MacDonald, *Nat. Mater.* **19**, 1265 (2020).
- [11] G. Tarnopolsky, A. J. Kruchkov, and A. Vishwanath, *Phys. Rev. Lett.* **122**, 106405 (2019).
- [12] P. Moon, M. Koshino, and Y.-W. Son, *Phys. Rev. B* **99**, 165430 (2019).
- [13] B. Huang and W. V. Liu, *Phys. Rev. B* **100**, 144202 (2019).
- [14] K. Hayashida, T. Dotera, A. Takano, and Y. Matsushita, *Phys. Rev. Lett.* **98**, 195502 (2007).
- [15] J. Zhang and F. S. Bates, *J. Am. Chem. Soc.* **134**, 7636 (2012).
- [16] T. M. Gillard, S. Lee, and F. S. Bates, *Proc. Natl. Acad. Sci.* **113**, 5167 (2016).
- [17] A. Jayaraman, C. M. Baez-Cotto, T. J. Mann, and M. K. Mahanthappa, *Proc. Natl. Acad. Sci.* **118**, e2101598118 (2021).
- [18] S. Fischer, A. Exner, K. Zielske, J. Perlich, S. Deloudi, W. Steurer, P. Lindner, and S. Förster, *Proc. Natl. Acad. Sci.* **108**, 1810 (2011).
- [19] C. Xiao, N. Fujita, K. Miyasaka, Y. Sakamoto, and O. Terasaki, *Nature* **487**, 349 (2012).
- [20] Y. E. Kraus, Z. Ringel, and O. Zeitler, *Phys. Rev. Lett.* **111**, 226401 (2013).
- [21] D.-T. Tran, A. Dauphin, N. Goldman, and P. Gaspard, *Phys. Rev. B* **91**, 085125 (2015).
- [22] C.-B. Hua, R. Chen, B. Zhou, and D.-H. Xu, *Phys. Rev. B* **102**, 241102 (2020).
- [23] Y. Chan, C. T. Chan, and Z. Liu, *Phys. Rev. Lett.* **80**, 956 (1998).
- [24] M. Kaliteevski, S. Brand, R. Abram, T. Krauss, R. D. Rue, and P. Millar, *Nanotechnology* **11**, 274 (2000).
- [25] M. Zoorob, M. Charlton, G. Parker, J. Baumberg, and M. Netti, *Nature* **404**, 740 (2000).
- [26] Z. Feng, X. Zhang, Y. Wang, Z.-Y. Li, B. Cheng, and D.-Z. Zhang, *Phys. Rev. Lett.* **94**, 247402 (2005).
- [27] W. Man, M. Megens, P. J. Steinhardt, and P. M. Chaikin, *Nature* **436**, 993 (2005).
- [28] R. C. Gauthier and K. Mnaymneh, *Opt. Express* **13**, 1985 (2005).
- [29] K. Nozaki and T. Baba, *Jpn. J. Appl. Phys.* **45**, 6087 (2006).
- [30] J. Ren, X. Sun, and S. Wang, *Opt. Laser Technol.* **101**, 42 (2018), ISSN 0030-3992.
- [31] X. Xi and X. Sun, *Superlattices Microstruct.* **129**, 247 (2019), ISSN 0749-6036.
- [32] S. Aubry and G. André, *Ann. Israel Phys. Soc.* **3**, 18 (1980).
- [33] Y. Lahini, R. Pugatch, F. Pozzi, M. Sorel, R. Morandotti, N. Davidson, and Y. Silberberg, *Phys. Rev. Lett.* **103**, 013901 (2009).
- [34] S. Ganeshan, K. Sun, and S. Das Sarma, *Phys. Rev. Lett.* **110**, 180403 (2013).
- [35] G. Domínguez-Castro and R. Paredes, *Eur. J. Phys.* **40**, 045403 (2019).
- [36] S. Longhi, *Phys. Rev. Lett.* **122**, 237601 (2019).
- [37] B. Simon, *Adv. Appl. Math.* **3**, 463 (1982).
- [38] J. Bellissard, A. Bovier, and J.-M. Ghez, *Rev. Math. Phys.* **4**, 1 (1992).
- [39] J.-M. Gambaudo and P. Vignolo, *New J. Phys.* **16**, 043013 (2014).
- [40] D. Tanese, E. Gurevich, F. Baboux, T. Jacqmin, A. Lemaître, E. Galopin, I. Sagnes, A. Amo, J. Bloch, and E. Akkermans, *Phys. Rev. Lett.* **112**, 146404 (2014).
- [41] G. Roati, C. D'Errico, L. Fallani, M. Fattori, C. Fort, M. Zaccanti, G. Modugno, M. Modugno, and M. Inguscio, *Nature* **453**, 895 (2008).
- [42] V. Goblot, A. Štrkalj, N. Pernet, J. L. Lado, C. Dorow, A. Lemaître, L. Le Gratiet, A. Harouri, I. Sagnes, S. Ravets, et al., *Nat. Phys.* **16**, 832 (2020).
- [43] K. Ueda and H. Tsunetsugu, *Phys. Rev. Lett.* **58**, 1272

- (1987).
- [44] A. Szabó and U. Schneider, Phys. Rev. B **101**, 014205 (2020).
- [45] R. Gautier, H. Yao, and L. Sanchez-Palencia, Phys. Rev. Lett. **126**, 110401 (2021).
- [46] Z. Zhu, S. Yu, D. Johnstone, and L. Sanchez-Palencia, arXiv p. 2307.09527 (2023).
- [47] D. Damanik and A. Gorodetski, Commun. Math. Phys. **305**, 221 (2011).
- [48] A. Sütő, J. Stat. Phys. **56**, 525 (1989).
- [49] S. He and J. Maynard, Phys. Rev. Lett. **62**, 1888 (1989).
- [50] Z. V. Vardeny, A. Nahata, and A. Agrawal, Nat. Photonics **7**, 177 (2013).
- [51] P. Wang, Q. Fu, V. V. Konotop, Y. V. Kartashov, and F. Ye, Nature Photonics **224**, 18 (2024).
- [52] L. Levi, M. Rechtsman, B. Freedman, T. Schwartz, O. Manela, and M. Segev, Science **332**, 1541 (2011).
- [53] Ş. Özdemir, S. Rotter, F. Nori, and L. Yang, Nat. Mater. **18**, 783 (2019).
- [54] Q. Lin, T. Li, L. Xiao, K. Wang, W. Yi, and P. Xue, Phys. Rev. Lett. **129**, 113601 (2022).
- [55] Q.-B. Zeng, Y.-B. Yang, and Y. Xu, Phys. Rev. B **101**, 020201 (2020).
- [56] T. Li, Y.-S. Zhang, and W. Yi, Phys. Rev. B **105**, 125111 (2022).
- [57] A. Padhan, S. R. Padhi, and T. Mishra, Phys. Rev. B **109**, L020203 (2024), URL <https://link.aps.org/doi/10.1103/PhysRevB.109.L020203>.
- [58] Z.-H. Xu, X. Xia, and S. Chen, Sci. China: Phys., Mech. Astron. **65**, 227211 (2022).
- [59] P. Sarnak, Commun. Math. Phys. **84**, 377 (1982).
- [60] J. Gea-Banaclóche, Y.-q. Li, S.-z. Jin, and M. Xiao, Phys. Rev. A **51**, 576 (1995).
- [61] Z. Zhang, F. Li, G. Malpuech, Y. Zhang, O. Bleu, S. Konikhin, C. Li, Y. Zhang, M. Xiao, and D. D. Solnyshkov, Phys. Rev. Lett. **122**, 233905 (2019), URL <https://link.aps.org/doi/10.1103/PhysRevLett.122.233905>.
- [62] Z. Zhang, S. Liang, F. Li, S. Ning, Y. Li, G. Malpuech, Y. Zhang, M. Xiao, and D. Solnyshkov, Optica **7**, 455 (2020).
- [63] Z. Zhang, Y. Feng, S. Ning, G. Malpuech, D. Solnyshkov, Z. Xu, Y. Zhang, and M. Xiao, Photonics Res. **10**, 958 (2022).
- [64] See Supplemental Material at [xURL will be inserted by publisher].
- [65] Z. Zhang, R. Wang, Y. Zhang, Y. V. Kartashov, F. Li, H. Zhong, H. Guan, K. Gao, F. Li, Y. Zhang, et al., Nat. Commun. **11**, 1902 (2020), ISSN 2041-1723.
- [66] Y. Feng, Z. Liu, F. Liu, J. Yu, S. Liang, F. Li, Y. Zhang, M. Xiao, and Z. Zhang, Phys. Rev. Lett. **131**, 013802 (2023).
- [67] B. S. Everitt and D. J. Hand, *Finite mixture distributions* (London: Chapman and Hall, 1981).
- [68] The special localization point visible in Fig. 2d for  $I_2/I_0 \approx 0.3$  occurs because some localized states appear in a perturbed periodic potential even before the fractalization of the energy spectrum. If the probe has a strong overlap with such state, the wavepacket will not expand, even though there are still propagative states available in some bands: they are simply not excited efficiently. The recovery of the expansion with the increase of the second lattice potential  $I_2$  confirms the occasional nature of this localization. On the contrary, the expansion is definitively suppressed once the true localization threshold is passed.
- [69] E. Miyai, K. Sakai, T. Okano, W. Kunishi, D. Ohnishi, and S. Noda, Nature **441**, 946 (2006).
- [70] B. Perez-Garcia, C. López-Mariscal, R. I. Hernandez-Aranda, and J. C. Gutiérrez-Vega, Appl. Opt. **56**, 6967 (2017).
- [71] Q. Fu, P. Wang, C. Huang, Y. V. Kartashov, L. Torner, V. V. Konotop, and F. Ye, Nature Photonics **14**, 663 (2020).
- [72] C. Jin, B. Cheng, B. Man, Z. Li, D. Zhang, S. Ban, and B. Sun, Appl. Phys. Lett. **75**, 1848 (1999).
- [73] E. Di Gennaro, D. Morello, C. Miletto, S. Savo, A. Andreone, G. Castaldi, V. Galdi, and V. Pierro, Photonics Nanostruct. **6**, 60 (2008).